sustainability

Article

Seismic Overturning Fragility Analysis for Rigid Blocks Subjected to Floor Motions

Hanquan Liu [1], Yong Huang [2,3] and Xiaohui Liu [1,*]

[1] Institute of Engineering Mechanics, China Earthquake Administration, No. 1 Chaobai Street, Sanhe 065201, China
[2] Key Lab of Structural Dynamic Behavior and Control of the Ministry of Education, School of Civil Engineering, Harbin Institute of Technology, 73 Huanghe Road, Harbin 150090, China
[3] Key Lab of Smart Prevention and Mitigation of Civil Engineering Disasters of the Ministry of Industry and Information Technology, Harbin Institute of Technology, 73 Huanghe Road, Harbin 150090, China
* Correspondence: liuxiaohui.iem@gmail.com

Abstract: This paper investigates the seismic rocking-overturning fragility of freestanding rigid blocks subjected to one-sine acceleration pulses from a probabilistic perspective. An equivalent single-degree-of-freedom (SDOF) model with a bespoke discrete damper is used to simulate the responses of four blocks with varying geometries under excitation with various characteristics. The simulation results are used to perform an overturning fragility analysis and evaluate the performance of various intensity measures (*IM*s). An *IM* strip, referred to as a hybrid strip, can be observed in the analysis, within which both safe rocking and overturning occur. For *IM* values outside of the hybrid strip, there exists a clear distinction between these two states. In this study, we introduce the hybrid ratio, a parameter that can estimate the size of the hybrid strip of different *IM*s. The hybrid ratio is defined as the combination of two ratios of hybrid strip width and the two *IM* strip widths corresponding to safe rocking and overturning, respectively. The effect of the different analysis strip widths is also examined in the overturning fragility analysis. The results suggest that the *IM* determined by excitation magnitude, frequency, and block geometry parameters demonstrates its superiority compared with some well-known *IM*s by having the smallest hybrid ratio and coefficient of variation, as well as good robustness of the overturning fragility curves against the change of the analysis strip width.

Keywords: rigid blocks; overturning; fragility; rocking response; intensity measure; dispersion; coefficient of variation

Citation: Liu, H.; Huang, Y.; Liu, X. Seismic Overturning Fragility Analysis for Rigid Blocks Subjected to Floor Motions. *Sustainability* **2023**, *15*, 4945. https://doi.org/10.3390/su15064945

Academic Editors: Yutao Pang, Junsheng Su, Xiaohui Yu and Xiyin Zhang

Received: 24 January 2023
Revised: 26 February 2023
Accepted: 8 March 2023
Published: 10 March 2023

1. Introduction

Building contents damage, an important part of earthquake-induced damage, has been attracting more and more interest from investigators since it was found that severe contents damage usually causes more significant financial loss compared with structural damage [1]. In the field of earthquake engineering, unanchored building contents are typically idealized as freestanding rigid blocks. During earthquake events, the motion of rigid blocks may be dominated by complex modes (e.g., sliding, twisting, rocking). During these complex motions, the blocks may impact each other or neighboring walls, and may even overturn. Among the dominating modes, rocking and sliding have attracted the most concern from investigators. Shenton [2] proposed an approach to distinguish different dominating modes of unanchored rigid blocks. The research addressing the sliding response can be found in the literature [3–10]. This study focuses on the rocking-overturning response of the freestanding rigid block, characterized by a partial bottom uplift and changing rotation center. The block can overturn when it undergoes a large enough rocking rotation.

As a pioneering work, the seminal framework proposed by Housner [11] for the seismic response evaluation of freestanding rigid blocks has been followed by many investigators, including experimental [12–20] and numerical efforts [21–33]. To predict the occurrence of overturning, Ishiyama [34] proposed overturning criteria involving the overturning acceleration and velocity, which are the minimum peak acceleration and velocity of the input excitation needed to overturn a rigid block, respectively. Kaneko and Hayashi [35] rearranged Ishiyama's equation [34] to obtain the overturning acceleration considering the frequency of the input excitation. Then, Kaneko and Hayashi [36] proposed an equation to determine the relationship between the overturning ratio and the input excitation. Kuo et al. [37] proposed seismic evaluation criteria for the clutter response of medicine shelves via shake table tests. Similarly, Zhang and Makris [38] analyzed the condition of overturning and derived an overturning acceleration spectrum, which has been widely used in rocking-overturning research [39,40]. However, the above deterministic views and methods to predict overturning seem to be inconsistent with reality, as the rocking motion is an extremely complex dynamic process, and the rocking response is barely "non-repeatable" [41–44]. Even minor adjustments of excitation or block geometry parameters may lead to significant differences of the response. This can be primarily attributed to the negative stiffness exhibited by the blocks [45] and the complex variability in energy dissipation [46]. Following the probabilistic point of view [42], fragility analysis, a commonly utilized approach in earthquake engineering [47], has been employed by numerous investigators [48–50] to evaluate the seismic performance of rigid blocks. This approach involves assessing a conditional probability for a damage measure exceeding a certain capacity limit state, given an *IM* value [51–53].

For assessing the rocking-overturning fragility, an incremental dynamic analysis (IDA)-based assessment method for the blocks subjected to floor motions is proposed by Liu et al. [54]. Nevertheless, rocking IDA curves generally differ from those of structural systems due to the frequent appearance of resurrections, the highly weaving non-monotonic behavior and the overall high variability [55], which presents new challenges to the application of IDA-pertinent approaches. Besides the IDA-based method, the maximum likelihood estimation (MLE) approach has been used to calculate the fragility function parameters for which the assumed statistical distribution attains the highest likelihood of producing the observed data [56]. Correspondingly, for a rocking-overturning fragility analysis, various *IM*s, including univariate *IM*s [57,58] and bivariate ones [56], have been proposed. A novel dimensionless *IM*, determined by the excitation magnitude, frequency, and block geometry parameters, was presented by Liu et al. [59] for evaluating the seismic rocking fragility, which demonstrates a closer correlation with the maximum rocking angle, thus achieve less dispersion of the fragility functions.

This paper takes a probabilistic insight into the rocking-overturning responses and evaluates the ability of a suite of *IM*s to describe the rocking-overturning response. The likelihood of overturning due to rocking is expressed with a 'categorical' response variable. In particular, a zero-valued (0) or one-valued (1) parameter suffices to describe overturning, because the rocking block either overturns or not [56]. The simulation of the rocking blocks is conducted using a reliable numerical model [60]. There exists a hybrid *IM* strip within which both overturning and safe rocking occur. For *IM* values outside of the hybrid strip, there exists a clear distinction between these two states. From the point of view of the hybrid strip, the hybrid ratio is proposed in this paper to quantitively compare the performance of various *IM*s in distinguishing the two states of safe rocking and overturning. Simulated overturning probabilities, the percentages of overturning occurrence within the specific *IM* value (strip), are used to generate fragility curves. In addition, the least squares method is used to obtain the parameters of the fragility functions. A novel *IM* [59], used for the first time in an overturning fragility analysis, receives the smallest hybrid ratio and the smallest coefficient of variation compared with some well-known *IM*s. Finally, the effect of different analysis strip widths is also examined, and the results show that the overturning fragility curves have good robustness against the change of the analysis strip width.

The following is an outline of the remaining sections. Section 2 provides the equation of motion for the rocking block and presents a discretely damped SDOF model, which is utilized to solve the rocking response. The experimental results are utilized to validate the numerical model. Utilizing an overturning acceleration spectrum [38], Section 3 demonstrates the rocking-overturning responses. In Section 4, an overturning fragility analysis is conducted in terms of a suite of *IM*s. A novel *IM* first used in predicting overturning successfully demonstrates its superiority by comparing it with some well-known ones. The final section provides some concluding remarks. Appendix A contains the notations of the variables utilized in the analysis.

2. Seismic Response of Rigid Blocks

2.1. Numerical Modeling

Consider a homogenous freestanding rectangular rigid block (Figure 1) that has the dimensions $2b \times 2h$, mass m. The center-of-mass (CM) of such a block coincides with its center-of-geometric. The block's geometry can be fully described using two parameters: the size parameter $R = \sqrt{b^2 + h^2}$ and the slenderness parameter, $\alpha = \text{atan}(b/h)$. Assume that the coefficient of friction between the block and its rigid base is big enough so that rocking (including overturning when the rocking angle is too large) is the only dominating mode. Its rotational moment of inertia to the pivot point O or O′ is $I_O = \frac{4}{3}mR^2$. In the simplest case, this system is SDOF.

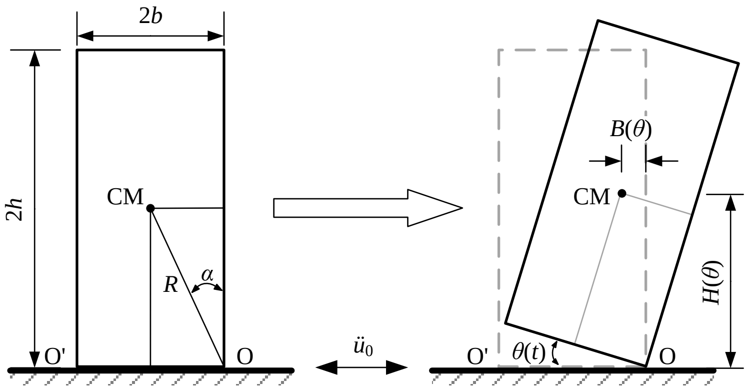

Figure 1. Rocking block geometry.

Assuming that there is no jump and, as a result, the rigid block remains at the same position at the instant of impact, the equation of motion of an undamped freestanding block in Figure 1 can be expressed by:

$$I_O\ddot{\theta} - m\ddot{u}_0 H(\theta) + mgB(\theta) = 0 \tag{1}$$

where θ is the rotation angle, $\ddot{u}_0$ is the horizontal excitation and g is the gravity acceleration. The line connecting the current pivot point and the CM can be decomposed into vertical and horizontal components, i.e., $H(\theta)$ and $B(\theta)$, respectively (Equations (2) and (3)):

$$H(\theta) = R\cdot \cos[\alpha\cdot \text{sgn}(\theta) - \theta] \tag{2}$$

$$B(\theta) = R\cdot \sin[\alpha\cdot \text{sgn}(\theta) - \theta] \tag{3}$$

where sgn() is the sign function.

There is a threshold for the horizontal excitation acceleration $\ddot{u}_0$ to cause the block to start rocking (Equation (4)). The restoring moment M can be uniquely determined by θ in Equation (5).

$$\ddot{u}_0 \geq gb/h = g\cdot \tan\alpha \tag{4}$$

$$M = mgR\sin[\alpha\cdot \text{sgn}(\theta) - \theta] \tag{5}$$

To simulate the rocking responses, we adopt an equivalent lumped mass SDOF model [61]. Figure 2 displays the equivalent representation of a rocking block (Figure 2a) as an SDOF oscillator (Figure 2b). The equation of motion for such an oscillator subjected to a floor motion $\ddot{u}_0$ is given by,

$$I_O\ddot{\theta} + f_d\left(\dot{\theta}\right) + k(\theta)\cdot\theta = -I_O\frac{\ddot{u}_0\cos\alpha}{R} \tag{6}$$

where $I_O = \frac{4}{3}mR^2$ is the moment of inertia, f_d is the damping force and k is the tangent stiffness of the rotational spring to model the restoring moment of the rocking block. $I_{CM} = \frac{mR^2}{3}$ is the additional moment of inertia to achieve the total moment of inertia I_O. To approximate the energy dissipation during rocking, a discrete damping force $f_d\left(\dot{\theta}\right)$ proposed by Liu et al. [60] is implemented in this SDOF model. In this discrete damping model the viscous damping force $f_d = c_D\dot{\theta}$ has a limited application range of $\pm\delta\alpha$ around the original position $\theta = 0$. Beyond this range, the damping force is set to 0. Therefore, the energy dissipation during rocking occurs solely when the system traverses its original position (Equation (7)):

$$f_d\left(\theta,\dot{\theta}\right) = \begin{cases} c_D\dot{\theta}, & |\theta| \le \delta\alpha \\ 0, & |\theta| > \delta\alpha \end{cases} \tag{7}$$

where c_D is a nonconstant discrete viscous damping coefficient proportional to the angular velocity $\dot{\theta}$ before each impact (Figure 3) expressed by Equation (8).

$$c_D = \frac{I_O}{2\delta\alpha}(1-e)\left|\dot{\theta}_1\right| \tag{8}$$

where e is the restitution coefficient of the rocking block, which is defined as the ratio of the angular velocity after the impact to that before the impact floor [62], i.e., $e = \dot{\theta}_2/\dot{\theta}_1$, with $\dot{\theta}_1$ and $\dot{\theta}_2$ representing the angular velocity of the rocking block before and after the impact. Under Housner's assumptions [11], the rigid-body restitution coefficient e_R can be derived by the slenderness parameter α (Equation (9)). It is worth mentioning that the restitution coefficient e in the real world is usually smaller than e_R because of the localized nonlinearity of the colliding materials. To better match the real-world energy dissipation, the restitution coefficient in this study is assumed to be $e = 0.95e_R$. The numerical simulation was performed in OpenSees (Version 3.0.0) [63], a world-renowned finite element modeling platform for earthquake engineering. Further implemental details can be found in our former paper [60].

$$e_R = 1 - 1.5\sin^2\alpha \tag{9}$$

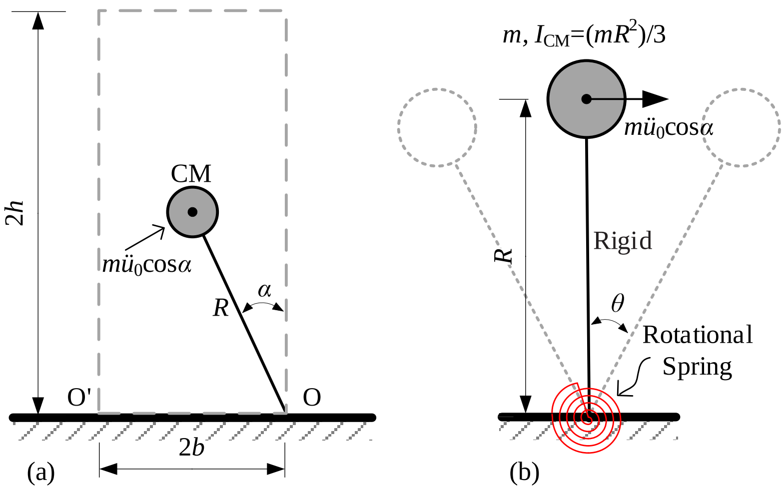

Figure 2. (**a**) Rigid block and (**b**) equivalent SDOF model.

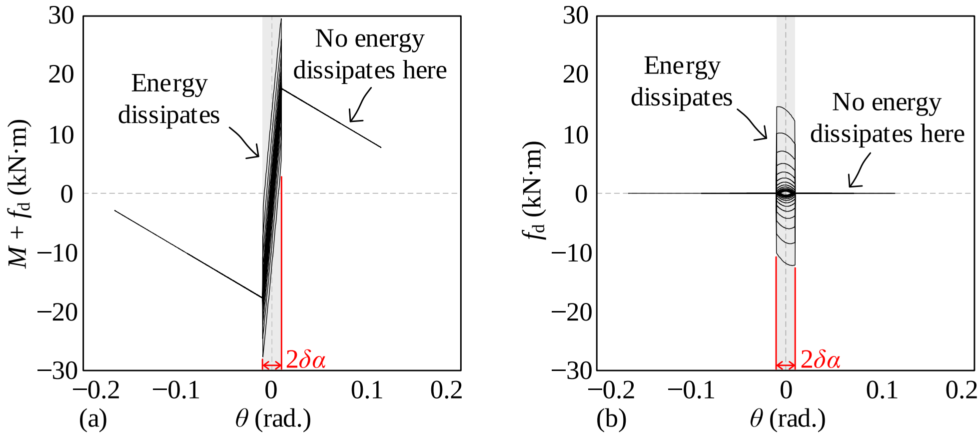

Figure 3. Hysteresis of the SDOF model: (**a**) total resisting moment vs. rocking angle, (**b**) damping force vs. rocking angle.

2.2. Experimental Verifications

The performance of the discrete damping model has been validated by a comparison with the experimental results of Nasi [64–66]. Figure 4 displays six selected runs of rotation-time history derived from the experiment and the simulation. The comparison shows that this numerical model with discrete damping can correctly approximate the maximum rocking angle and predict overturning [59,60].

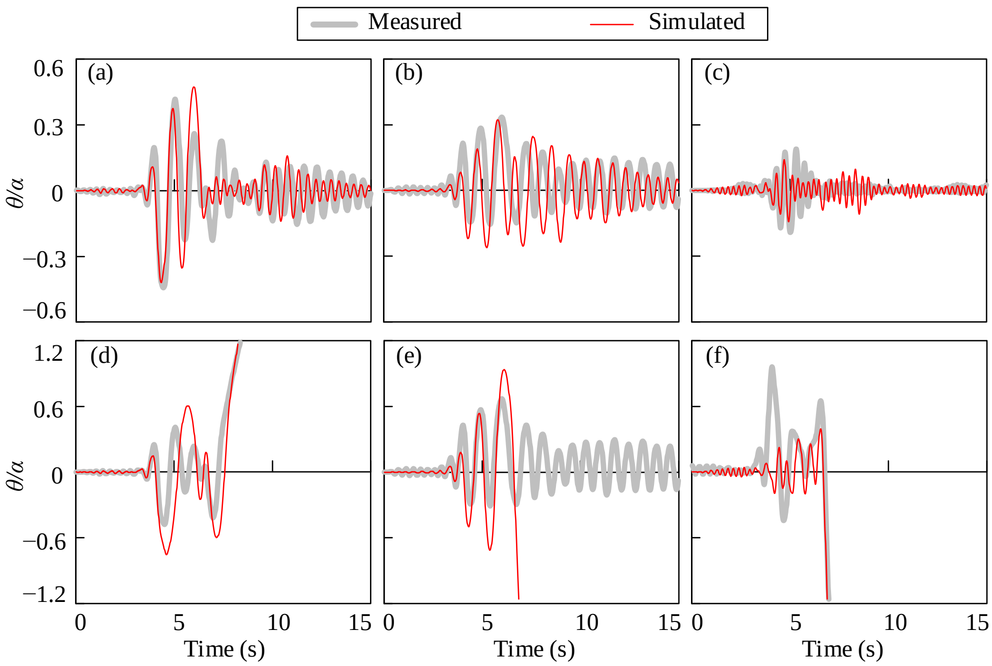

Figure 4. Rotation histories of safe rocking (**a**–**c**) and overturning (**d**–**f**).

3. Overturning Acceleration Spectrum

The response results of the rigid rocking blocks are usually studied in terms of the rocking spectrum. Zhang and Makris [38] presented a two-dimensional overturning acceleration spectrum, with two axes of ω_P/P, and $PFA/g\tan\alpha$. Here, ω_P is the circular frequency of the one-sine pulse acceleration excitation, $P = \sqrt{3g/4R}$ is a block frequency parameter proposed by Housner [11] and PFA is the peak floor acceleration. In this study, the overturning acceleration spectrum proposed by Zhang and Makris [38] is simplified by only dividing into the overturning and safe rocking zone. For the subsequent overturning fragility analysis, a set of data were generated based on the overturning acceleration spectrum. We selected four models of sizes of typical furniture or equipment (Figure 5).

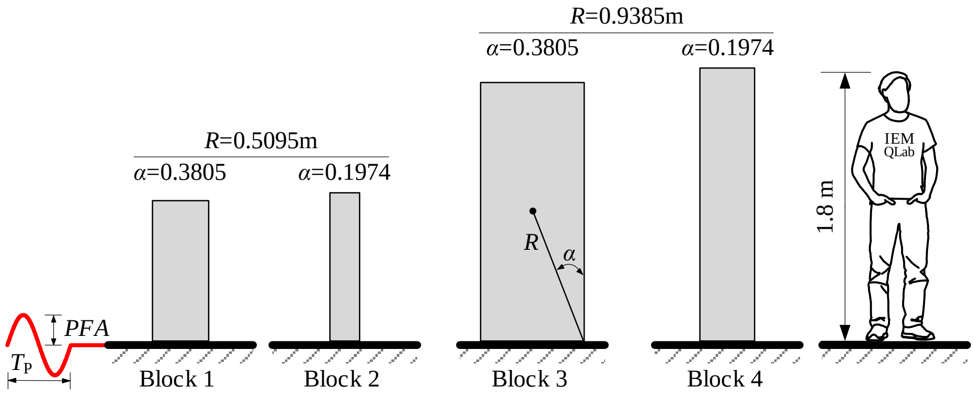

Figure 5. Investigated rocking blocks.

By exposing each model to 100 one-sine pulse excitations of different PFA and ω_P, we derived simulated results for 400 uniformly distributed cases (Figure 6a). A boundary can be observed between the overturning and safe area (Figure 6b), as Zhang and Makris [38] concluded. The occurrence of overturning corresponds to ω_P/P and $PFA/g\tan\alpha$, both widely-used *IM*s. However, using either one of these methods alone is insufficient for an overturning fragility analysis, highlighting the advantage of bivariate *IM*s [56]. Furthermore, this fact also consists of the motivation of this paper, which is that a good *IM* for an overturning fragility analysis should include as much of the excitation characteristics (e.g., PFA and ω_P) and the block geometry information (e.g., R and α), as mentioned in our former research [59].

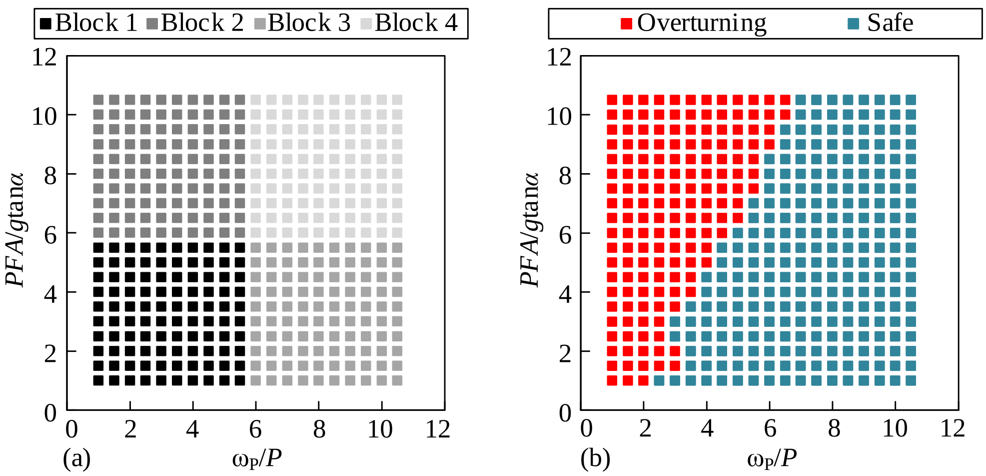

Figure 6. (**a**) Model distribution and (**b**) overturning spectrum.

It is worth noting that this study utilizes simple one-sine pulses as external excitations. Unlike rocking structures, building contents are subject to floor motion rather than ground motion. Previous work by D'Angela et al. [67] suggests that the input for freestanding bodies should better fit floor motion, and floor motions usually exhibit a relatively reduced record-to-record uncertainty. During earthquake events, the floor motion of a building is filtered by the structural system, resulting in dominant frequency components [68,69] (primarily related to the first natural frequency, or the first three natural frequencies). Although simplified motions may not fully capture the complexities of realistic floor motions under earthquake excitations, they do offer a foundation for understanding the response of rigid blocks and serve as a starting point for more sophisticated analyses.

4. Overturning Fragility Analysis

To determine the overturning fragility, one should first estimate the conditional probability P_f for the damage measure (DM) surpassing a pre-defined capacity limit state (LS), given an *IM* value:

$$P_f = P(DM > LS|IM) \tag{10}$$

To facilitates the calculation of conditional probability P_f, Dimitrakopoulos and Paraskeva [56] have presented a probability tree diagram that takes into account the peculiarities of the rocking responses (Figure 7). The probability P_f is calculated by combining two likelihoods, i.e., the rocking-overturning probability (P_{ro}) and the probability of DM surpassing LS without overturning (P_{ex}). As the probability P_{ex} during safe rocking has been studied [59], this paper focuses on deriving the overturning probability P_{ro}, and a comparative study of a suite of *IM*s has been conducted on the performance of deriving the overturning probability.

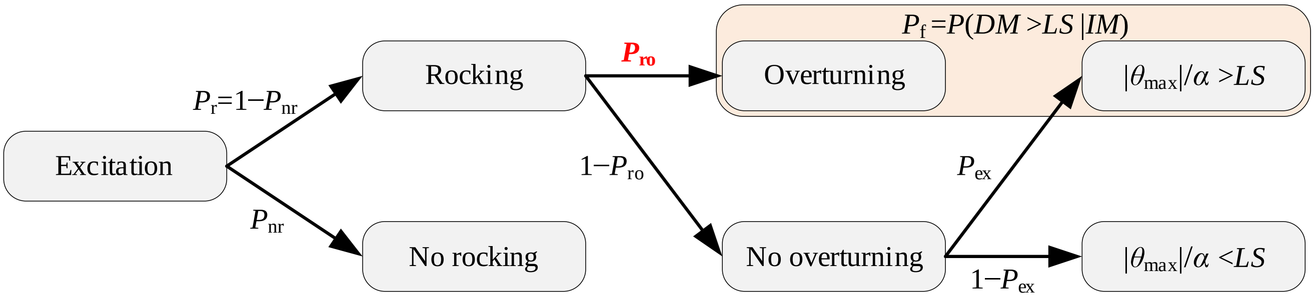

Figure 7. Probability tree diagram for the rocking problem.

4.1. Damage Measure and Limit States

In the real world, it is obvious that overturning occurs when the absolute peak rocking rotation $|\theta_{max}|$ reaches $\pi/2$. In the subsequent overturning fragility analysis, $|\theta_{max}|$ is used as the DM in this paper and LS = $\pi/2$ indicates the occurrence of overturning (Equation (11)).

$$DM = |\theta_{max}|, \quad LS = \pi/2 \tag{11}$$

The dimensionless DM, normalized absolute peak rocking angle $|\theta_{max}|/\alpha$, has been widely adopted for rocking fragility analysis because it provides a straight insight into the degree of rocking response [56–59]. Its physical meaning is clear: a larger-than-zero value implies the existence of rocking, whereas higher values indicate more severe rocking and even overturning. This index ($|\theta_{max}|/\alpha$) is also used as a criteria of overturning, but there are different opinions on the threshold value. Some investigators use larger-than-one values to denote overturning [54,58,70], while some other researchers have suggested the possibility of the block surviving overturning and returning to its original configuration eventually with $|\theta_{max}|/\alpha > 1.0$ [38,71], which differs from the common quasi-static viewpoint of the seismic response. When overturning occurs the numerical response may tend to infinite values. Thus, Dimitrakopoulos and Paraskeva [56] pointed out that the threshold of overturning does not correspond to a particular rotation value (e.g., $|\theta_{max}|/\alpha > 1.0$ or even 1.5), but rather at infinite values in numerical simulations.

4.2. Intensity Measures

Liu et al. [59] evaluated eight frequently used dimensionless *IM*s in a rocking fragility analysis and proposed a novel dimensionless *IM* determined by the excitation magnitude, frequency and block geometry parameters. The novel *IM* shows obvious superiority in predicting the peak rocking rotation angle during safe rocking compared with eight well-known *IM*s. In this paper, we use the same *IM* suite to evaluate their performance in an overturning analysis. The detailed information on the *IM* suite is listed in Table 1 and can also be found in [59].

Table 1. Detailed information on the *IM* suite.

Intensity Measure	Expression	Physical Meaning	Ref
IM_1	$\frac{\omega_P}{P}$	Dimensionless excitation frequency	[38]
IM_2	$\frac{PFA}{g\tan\alpha}$	Dimensionless PFA	[38]
IM_3	$\frac{P\cdot PFV}{g\tan\alpha}$	Dimensionless PFV	[56]
IM_4	$1.484\left(\frac{PFA}{g\tan\alpha}\right)^{1.644}\left(\frac{\omega_P}{P}\right)^{-2.013}$	Dimensionless combinations of PFA and floor motion frequency	[56]
IM_5	$0.063\left(\frac{PFA}{g\tan\alpha}\right)^{2.954}\left(\frac{\omega_P}{P}\right)^{-0.942}$		[56]
IM_6	$\left(\frac{PFA}{g\tan\alpha}\right)^{0.52}\left(\frac{\omega_P}{P}\right)^{-0.48}$		[56]
IM_7	$\left(\frac{PFA}{g\tan\alpha}\right)^{0.6}\left(\frac{\omega_P}{P}\right)^{-0.4}$		[56]
IM_8	$\frac{{e_R}^4\cdot P\cdot PFV}{g\tan\alpha}$	Dimensionless PFV considering the restitution coefficient	[58]
IM_9	$\frac{PFA\cdot {T_P}^2}{R\tan\alpha}$ *	Dimensionless floor displacement	[59]

* T_P is the period of the one-sine pulse excitation.

Within this *IM* suite, IM_1 to IM_3 are univariate *IM*s with the physical meaning of dimensionless excitation frequency, dimensionless PFA and dimensionless PFV, respectively. IM_4 to IM_7 are bivariate *IM*s, which may increase the computational cost. IM_8 is an *IM* proposed by Sieber et al. [58] with the physical meaning of the dimensionless peak velocity considering the restitution coefficient e_R. The novel IM_9 [59], with the physical meaning of dimensionless displacement, explicitly considers the excitation (PFA and ω_P) and the block geometric (R and α).

4.3. Hybrid Strip and Hybrid Ratio

Figure 8 displays the simulated rocking responses against the varying values of different *IM*s. There exists a particular hybrid *IM* strip (HS), within which both safe rocking and overturning occur, and outside of which a clear distinction can be made between the two states of safe rocking and overturning. To quantitively estimate the size of the HS, the hybrid ratio (HR) is presented in this paper to compare the performance of various *IM*s for predicting overturning (Figure 8). The parameter HR defined in Equation (12) can assess the performance of different *IM*s to evaluate whether a rigid block will overturn if subjected to an excitation.

$$HR = \sqrt{\left(\frac{W_{HS}}{R_S}\right)^2 + \left(\frac{W_{HS}}{R_O}\right)^2} \tag{12}$$

where W_{HS} is the width of the hybrid strip, R_S and R_O are the range of *IM* corresponding to safe rocking and the range of *IM* corresponding to overturning, respectively. Generally, a smaller HR for a type of *IM* indicates a smaller size of the hybrid strip relative to the overall *IM* range, which means a better prediction performance.

Figure 9 offers a comparative evaluation of all the examined *IM*s. The novel IM_9 is the closest to the origin of the coordinates, i.e., the HR of IM_9 is the smallest (Table 2). Although IM_1 has the smallest W_{HS}/R_S (0.50), IM_9 is close to it (0.51). These results indicate that IM_9 can best identify the state transition from safe rocking to overturning compared with the other eight *IM*s.

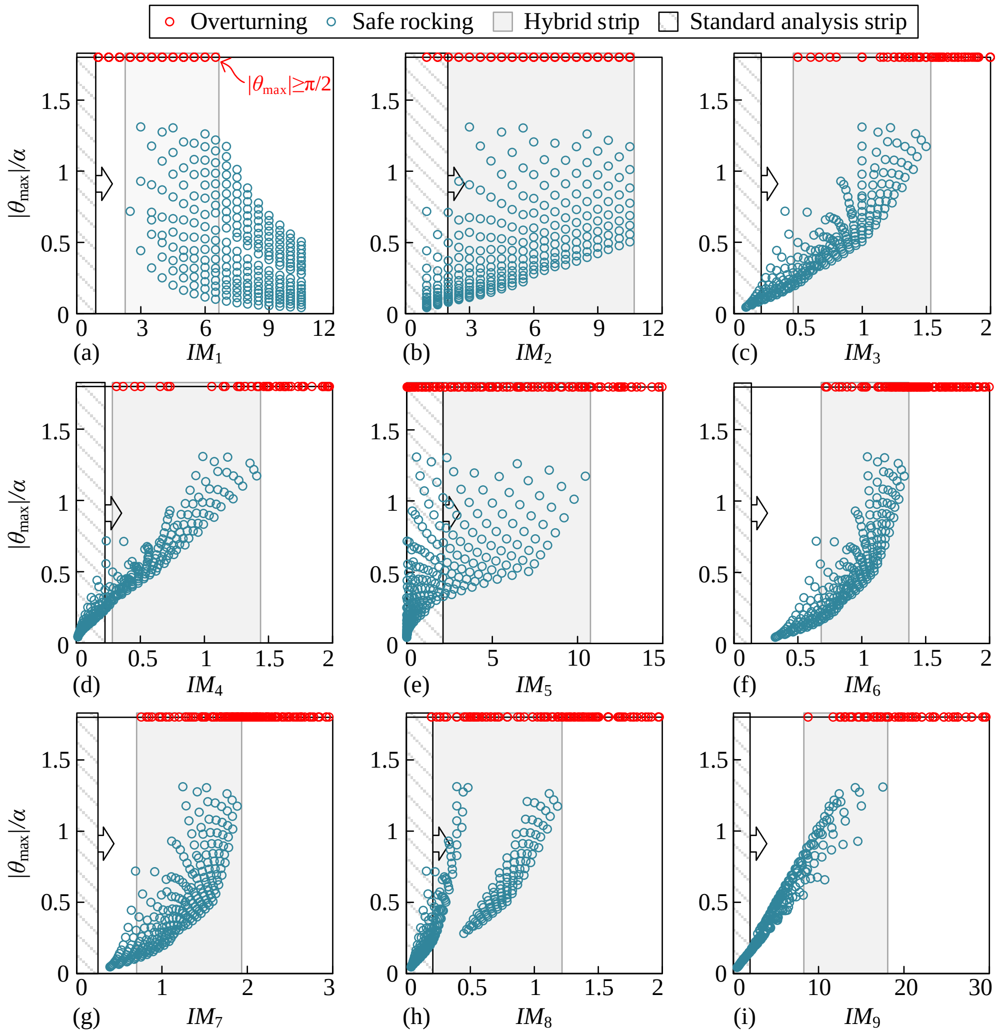

Figure 8. Seismic response analyses for different *IM*s.

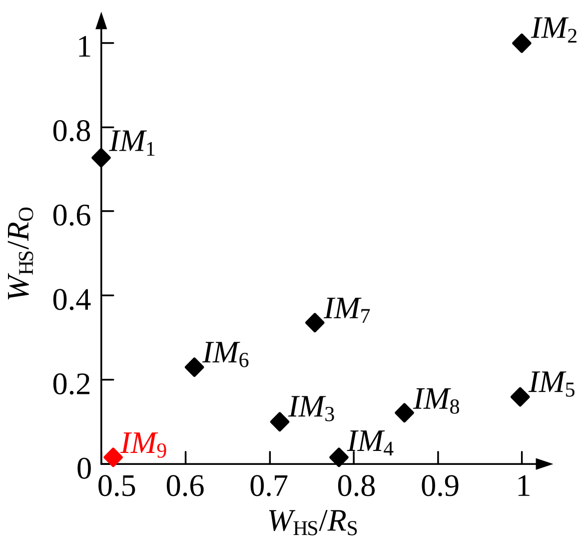

Figure 9. Comparative evaluation of different *IM*s.

Table 2. Analysis parameters of different *IM*s.

IM	W_{HS}	R_S	R_O	W_{HS}/R_S	W_{HS}/R_O	HR	W_{SAS}
IM_1	4.00	8.00	5.50	0.50	0.73	0.88	0.80
IM_2	9.50	9.50	9.50	1.00	1.00	1.41	1.90
IM_3	1.00	1.40	10.00	0.71	0.10	0.72	0.20
IM_4	1.09	1.40	70.52	0.78	0.02	0.78	0.20
IM_5	10.43	10.46	65.42	1.00	0.16	1.01	2.00
IM_6	0.62	1.01	2.68	0.61	0.23	0.65	0.12
IM_7	1.12	1.49	3.34	0.75	0.34	0.83	0.20
IM_8	0.98	1.14	8.08	0.86	0.12	0.87	0.19
IM_9	8.77	17.07	543.92	0.51	0.02	0.51	1.70

4.4. Probability of Overturning

The standard analysis strip (SAS), whose width (W_{SAS}) is one-fifth of W_{HS}, is used to obtain the overturning probability within the specific *IM* value in Figure 8. The overturning probability P_{ro} can be estimated directly by Equation (13), which can be used in the subsequent overturning fragility analysis to obtain the fragility curves.

$$P_{ro} = \frac{\text{number of overturning simulations}}{\text{total number of rocking simulations}} \tag{13}$$

The lognormal cumulative distribution function is widely used to fit fragility functions in earthquake engineering because of its robustness in deriving fragility functions [72]:

$$P(\text{Overturning}|IM = x) = \Phi\left(\frac{\ln(x/\mu)}{\beta}\right) \tag{14}$$

where P is the probability that excitation with $IM = x$ will cause the overturning of the rigid block, Φ is the standard normal cumulative distribution function, μ is the median of the fragility function (the *IM* level with a 50% probability of overturning), and β is the dispersion or logarithmic standard deviation. The least squares method is used to fit the overturning probability data obtained from Figure 8 to generate the overturning fragility curves. The error between the overturning probability data and the fitted overturning probability from the fragility function is:

$$error = \sum_{i=1}^{n} (P_i - P_{\text{fit}}(IM = x_i))^2 \tag{15}$$

where n is the number of the overturning probability data, P_i is the ith overturning probability and P_{fit} is the fitted overturning probability when the $IM = x_i$. The error can be minimized by adjusting β:

$$\beta = \text{argmin}(error) = \text{argmin} \sum_{i=1}^{n} \left(P_i - \Phi\left(\frac{\ln(x_i/\mu)}{\beta}\right)\right)^2 \tag{16}$$

Figure 10 shows the overturning fragility curves for different *IM*s obtained by fitting the overturning probability data. For comparing the performance of various *IM*s in estimating the overturning probability, the fitted analysis parameters are used to generate the coefficient of variation (CV) in this paper. CV is a standardized measure of the dispersion of a probability distribution defined as the ratio of the standard deviation β to the mean μ. Compared with the other eight *IM*s, IM_9 exhibits obvious superiority by having the smallest CV (Figure 11). Therefore, IM_9 is recommended as an *IM* for overturning fragility analysis.

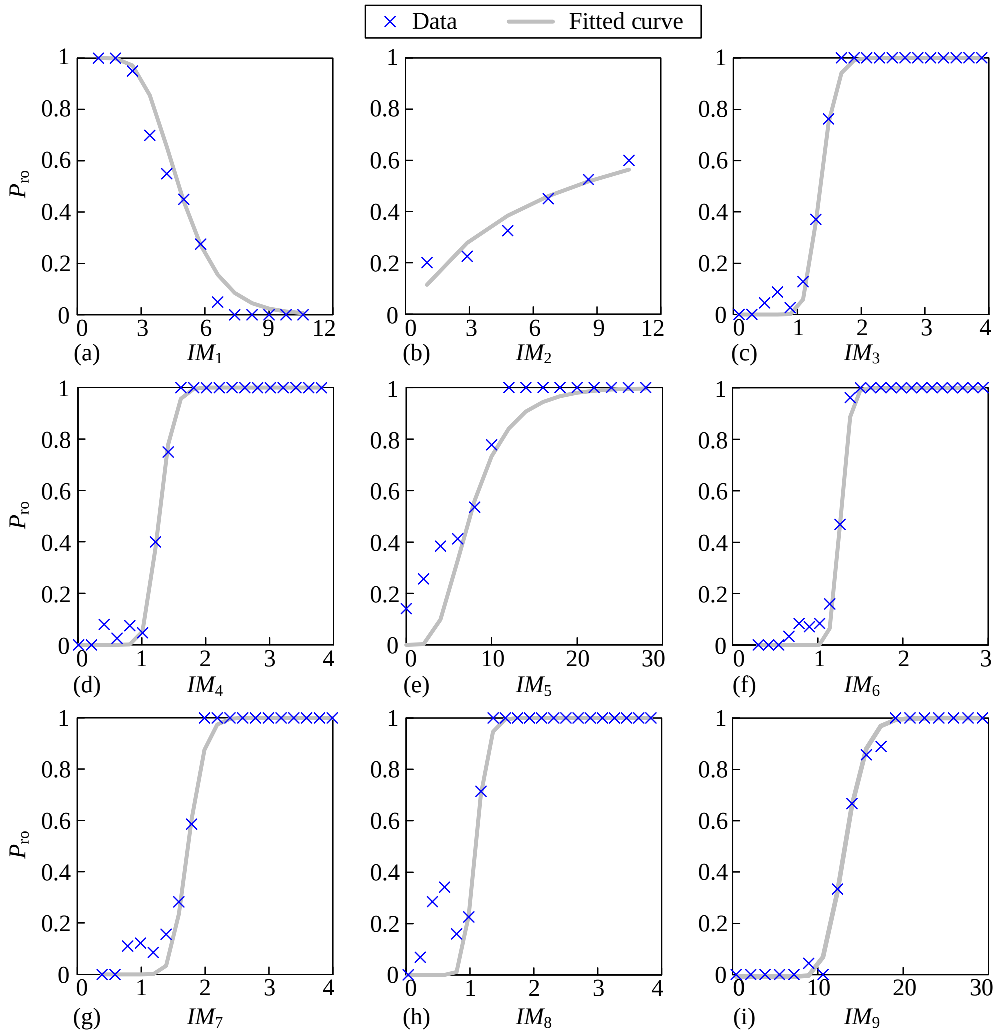

Figure 10. Overturning fragility curves for different *IM*s.

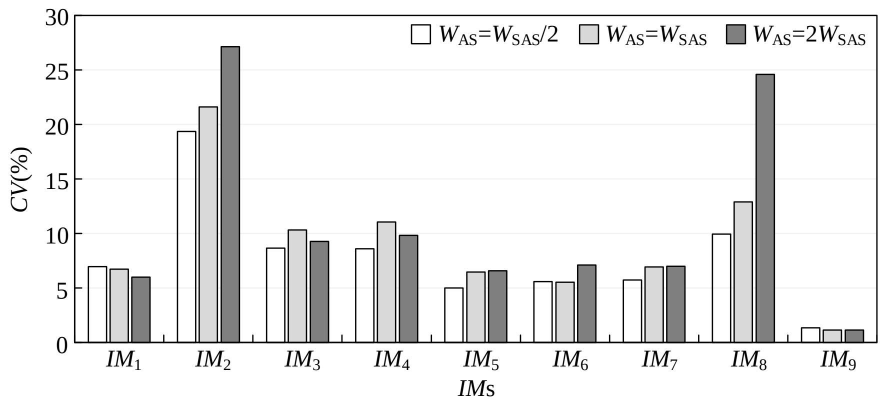

Figure 11. Coefficient of variation for different *IM*s.

4.5. Effect of Analysis Strip Width

From the process of an overturning fragility analysis, it can be found that the width of the analysis strip may affect the fragility curves. To examine this effect, we adjusted the width of the analysis strip (W_{AS}) to half and twice W_{SAS}, respectively. Figure 12 shows that, for all nine *IM*s, the overturning fragility curves obtained for different analysis strip widths are almost the same. The fragility curves have good robustness for different widths of the analysis strips. IM_9 maintains the smallest CV, which once again proves its superiority for overturning fragility analysis (Table 3).

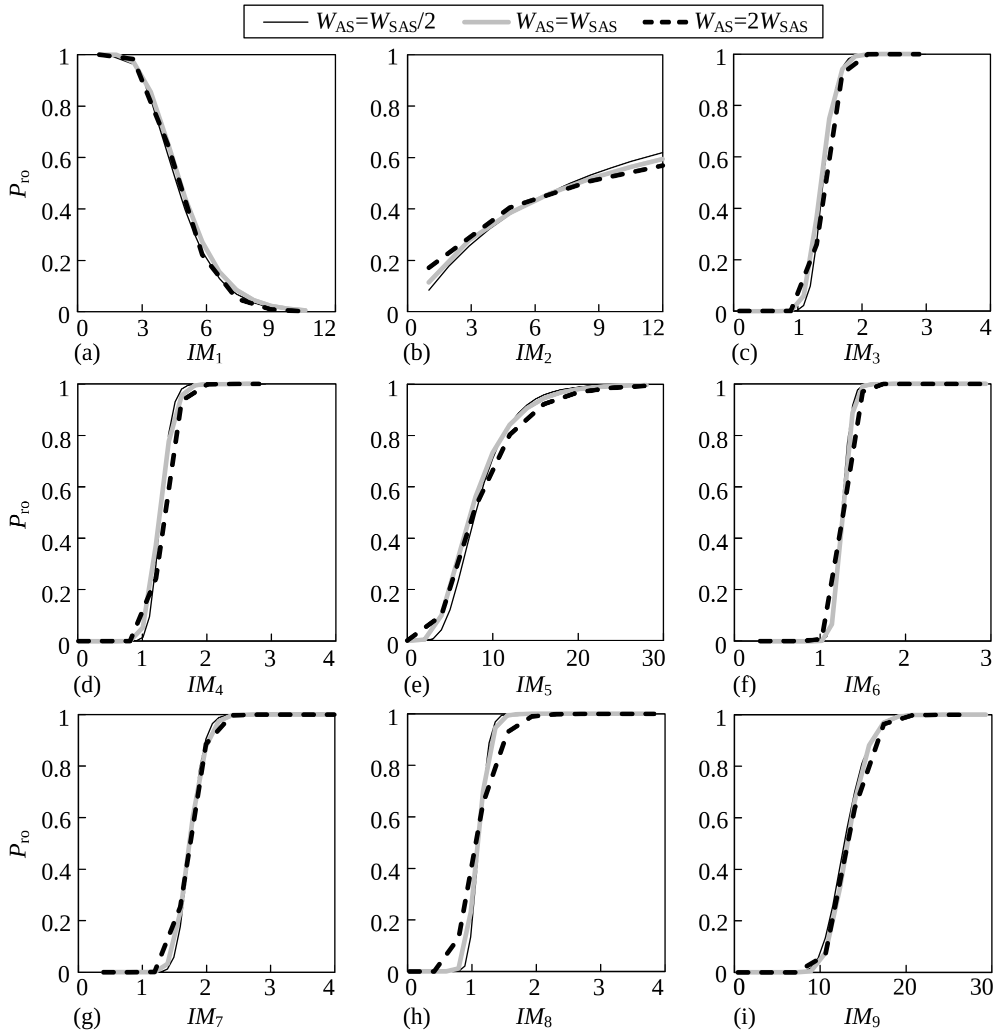

Figure 12. Overturning fragility curves for different widths of the analysis strips.

Table 3. Analysis parameters for different widths of the analysis strips.

IM	$W_{AS} = W_{SAS}/2$			$W_{AS} = W_{SAS}$			$W_{AS} = 2W_{SAS}$		
	μ	β	**CV (%)**	μ	β	**CV (%)**	μ	β	**CV (%)**
IM_1	4.60	0.32	6.96	4.77	0.32	6.71	4.68	0.28	5.98
IM_2	7.65	1.48	19.35	7.97	1.72	21.59	8.19	2.22	27.12
IM_3	1.39	0.12	8.63	1.36	0.14	10.32	1.40	0.13	9.27
IM_4	1.28	0.11	8.58	1.27	0.14	11.05	1.32	0.13	9.82
IM_5	8.01	0.40	5.00	7.43	0.48	6.46	7.76	0.51	6.57
IM_6	1.25	0.07	5.59	1.27	0.07	5.52	1.27	0.09	7.10
IM_7	1.74	0.10	5.73	1.73	0.12	6.92	1.72	0.12	6.97
IM_8	1.11	0.11	9.94	1.09	0.14	12.88	1.06	0.26	24.57
IM_9	12.80	0.17	1.33	13.15	0.15	1.14	13.28	0.15	1.13

5. Conclusions

This study provides deterministic and probabilistic views into the rocking-overturning responses of freestanding rigid blocks. The simulated results for four block models under excitation with various characteristics were conducted to generate the overturning spectrum. A comparative study of nine intensity measures, including one used for the first time in overturning fragility analysis was conducted to evaluate their capability to predict overturning. The overturning fragility curves were derived by the least-square fitting of a lognormal cumulative distribution. Some concluding remarks are drawn:

1. An effective *IM* for overturning fragility analysis should include as many of the excitation characteristics and as much of the block geometry information as possible.
2. A hybrid ratio, a parameter that can estimate the size of the hybrid *IM* strip within which both safe rocking and overturning may occur, is presented to quantitively compare the performance of various *IM*s in predicting overturning. A novel IM_9 (dimensionless floor displacement) had the best performance with the smallest HR.
3. The novel IM_9 first used in an overturning fragility analysis performs best by significantly reducing the coefficient of variation compared with some well-known *IM*s. Thus, IM_9 is recommended as an *IM* for overturning fragility analysis.
4. Different widths of analysis strips were used to generate the overturning fragility curves. The results show that the strip width only slightly affects the overturning fragility curves, thus revealing the good robustness of the analysis process.

Author Contributions: Conceptualization, H.L. and X.L.; methodology, H.L. and X.L.; software, H.L. and X.L.; validation, H.L. and X.L.; investigation, H.L., Y.H. and X.L.; writing—original draft preparation, H.L., Y.H. and X.L.; writing—review and editing, H.L., Y.H. and X.L. All authors have read and agreed to the published version of the manuscript.

Funding: This research received no external funding.

Acknowledgments: We thank Lucas Laughery for generously sharing the experimental data in their data paper published in 2018.

Conflicts of Interest: The authors declare no conflict of interest.

Appendix A

Table A1. Notations of the variable.

Symbol	Definition
$2b$	Width
$2h$	Height
R	Size parameter
α	Slenderness parameter
I_{O}	Moment of inertia
θ and $\ddot{\theta}$	Rotation angle and rotational angular acceleration
$\ddot{u}_0$	Horizontal excitation
H and B	Vertical and horizontal transient distances
g	Gravity acceleration
M	Restoring moment
$\dot{\theta}_1$ and $\dot{\theta}_2$	Angular velocities before and after impacts
e	Restitution coefficient
e_R	Rigid-body restitution coefficient
f_d	Damping force
k	Tangent stiffness
I_{CM}	Additional moment of inertia
$\delta\alpha$	Small range around initial position
c_D	Discrete viscous damping coefficient
$\theta_{\max}$	Peak rocking rotation
T_{p}	Period of pulse excitation
ω_{P}	Circular frequency of pulse excitation
P	Frequency parameter of block
PFA	Peak floor acceleration
PFV	Peak floor velocity
IM	Intensity measure
DM	Damage measure
LS	Limit state

Table A1. *Cont.*

Symbol	Definition
P_f	Conditional probability
P_{ro}	Overturning probability
P_{ex}	Probability of DM exceeding LS within safe rocking
W_{HS}	Width of the hybrid strip
R_{S} and R_{O}	*IM* range corresponding to safe rocking and overturning
HR	Hybrid ratio
W_{SAS}	Standard analysis strip width
P_i	Overturning probability
P_{fit}	Fitted overturning probability
β	Dispersion
μ	Median value of fragility function
CV	Coefficient of variation

References

1. Taghavi, S.; Miranda, M.M. *Response Assessment of Nonstructural Building Elements*; Pacific Earthquake Engineering Research Center: Berkeley, CA, USA, 2003.
2. Shenton, H.W., III. Criteria for initiation of slide, rock, and slide-rock rigid-body modes. *J. Eng. Mech.* **1996**, *122*, 690–693. [CrossRef]
3. Newmark, N.M. Effects of Earthquakes on Dams and Embankments. *Géotechnique* **1965**, *15*, 139–160. [CrossRef]
4. Garcia, D.L.; Soong, T.T. Sliding fragility of block-type nonstructural components. Part 1: Freestanding components. *Earthq. Eng. Struct. Dyn.* **2003**, *32*, 111–129. [CrossRef]
5. Chaudhuri, S.R.; Hutchinson, T.C. Characterizing frictional behavior for use in predicting the seismic response of unattached equipment. *Soil Dyn. Earthq. Eng.* **2005**, *25*, 591–604. [CrossRef]
6. Konstantinidis, D.; Makris, N. Experimental and analytical studies on the response of freestanding laboratory equipment to earthquake shaking. *Earthq. Eng. Struct. Dyn.* **2008**, *38*, 827–848. [CrossRef]
7. Gazetas, G.; Garini, E.; Berrill, J.B.; Apostolou, M. Sliding and overturning potential of Christchurch 2011 earthquake records. *Earthq. Eng. Struct. Dyn.* **2012**, *41*, 1921–1944. [CrossRef]
8. Nagao, T.; Kagano, H.; Hamaguchi, K. Full-scale shake table test on furnitures subjected to long-period earthquake motions. In Proceedings of the 15th World Conference on Earthquake Engineering, Lisbon, Portugal, 24–28 September 2012.
9. Konstantinidis, D.; Nikfar, F. Seismic response of sliding equipment and contents in base-isolated buildings subjected to broadband ground motions. *Earthq. Eng. Struct. Dyn.* **2014**, *44*, 865–887. [CrossRef]
10. Nikfar, F.; Konstantinidis, D. Peak Sliding Demands on Unanchored Equipment and Contents in Base-Isolated Buildings under Pulse Excitation. *J. Struct. Eng.* **2017**, *143*, 04017086. [CrossRef]
11. Housner, G.W. The behavior of inverted pendulum structures during earthquakes. *Bull. Seismol. Soc. Am.* **1963**, *53*, 403–417. [CrossRef]
12. Filiatrault, A.; Kuan, S.; Tremblay, R. Shake table testing of bookcase–partition wall systems. *Can. J. Civ. Eng.* **2004**, *31*, 664–676. [CrossRef]
13. Peña, F.; Prieto, F.; Lourenço, P.B.; Costa, A.C.; Lemos, J.V. On the dynamics of rocking motion of single rigid-block structures. *Earthq. Eng. Struct. Dyn.* **2007**, *36*, 2383–2399. [CrossRef]
14. Konstantinidis, D.; Makris, N. Experimental and analytical studies on the response of 1/4-scale models of freestanding laboratory equipment subjected to strong earthquake shake. *Bull. Earthq. Eng.* **2010**, *8*, 1457–1477. [CrossRef]
15. Bachmann, J.A.; Blöchlinger, P.; Wellauer, M.; Vassiliou, M.F.; Stojadinovic, B. Experimental investigation of the seismic response of a column rocking and rolling on a concave base. In Proceedings of the ECCOMAS Congress, VII European Congress on Computational Methods in Applied Sciences and Engineering, Crete Island, Greece, 5–10 June 2016; pp. 5023–5062.
16. Huang, B.; Pan, Q.; Lu, W.; Shen, F. Free-Rocking Tests of a Freestanding Object with Variation of Center of Gravity. *Earthq. Eng. Struct. Dyn.* **2021**, *50*, 3015–3040. [CrossRef]
17. Vassiliou, M.F.; Broccardo, M.; Cengiz, C.; Dietz, M.; Dihoru, L.; Gunay, S.; Mosalam, K.M.; Mylonakis, G.; Sextos, A.; Stojadinovic, B. Shake table testing of a rocking podium: Results of a blind prediction contest. *Earthq. Eng. Struct. Dyn.* **2020**, *50*, 1043–1062. [CrossRef]
18. Di Sarno, L.; Magliulo, G.; D'Angela, D.; Cosenza, E. Experimental assessment of the seismic performance of hospital cabinets using shake table testing. *Earthq. Eng. Struct. Dyn.* **2019**, *48*, 103–123. [CrossRef]
19. Vassiliou, M.F.; Cengiz, C.; Dietz, M.; Dihoru, L.; Broccardo, M.; Mylonakis, G.; Sextos, A.; Stojadinovic, B. Data set from shake table tests of free-standing rocking bodies. *Earthq. Spectra* **2021**, *37*, 2971–2987. [CrossRef]
20. Shang, Q.; Li, J.; Du, C.; Wang, T. Seismic Fragility Analysis of Freestanding Hospital Cabinets Based on Shaking Table Tests. *J. Earthq. Eng.* **2022**, 1–20. [CrossRef]

21. Chae, Y.B.; Kim, J.K. Implementation of configuration dependent stiffness proportional damping for the dynamics of rigid multi-block systems. *Earthq. Eng. Eng. Vib.* **2003**, *2*, 87–97. [CrossRef]
22. Di Egidio, A.; Zulli, D.; Contento, A. Comparison between the seismic response of 2D and 3D models of rigid blocks. *Earthq. Eng. Eng. Vib.* **2014**, *13*, 151–162. [CrossRef]
23. Vetr, M.G.; Nouri, A.R.; Kalantari, A. Seismic evaluation of rocking structures through performance assessment and fragility analysis. *Earthq. Eng. Eng. Vib.* **2016**, *15*, 115–127. [CrossRef]
24. Fragiadakis, M.; Kolokytha, M.; Diamantopoulos, S. Seismic risk assessment of rocking building contents of multistorey buildings. *Procedia Eng.* **2017**, *199*, 3534–3539. [CrossRef]
25. Gesualdo, A.; Iannuzzo, A.; Minutolo, V.; Monaco, M. Rocking of freestanding objects: Theoretical and experimental comparisons. *J. Theor. Appl. Mech.* **2018**, *56*, 977–991. [CrossRef]
26. Kasinos, S.; Lombardo, M.; Makris, N.; Palmeri, A. Dynamic response analysis of nonlinear secondary oscillators to idealised seismic pulses. *Earthq. Eng. Struct. Dyn.* **2020**, *49*, 1473–1495. [CrossRef]
27. Manzo, N.R.; Vassiliou, M.F. Simplified analysis of bilinear elastic systems exhibiting negative stiffness behavior. *Earthq. Eng. Struct. Dyn.* **2020**, *50*, 580–600. [CrossRef]
28. D'Angela, D.; Magliulo, G.; Cosenza, E. Towards a reliable seismic assessment of rocking components. *Eng. Struct.* **2020**, *230*, 111673. [CrossRef]
29. Aghagholizadeh, M. A finite element model for seismic response analysis of vertically-damped rocking-columns. *Eng. Struct.* **2020**, *219*, 110894. [CrossRef]
30. Vanin, F.; Penna, A.; Beyer, K. A three-dimensional macroelement for modelling the in-plane and out-of-plane response of masonry walls. *Earthq. Eng. Struct. Dyn.* **2020**, *49*, 1365–1387. [CrossRef]
31. Galvez, F.; Sorrentino, L.; Dizhur, D.; Ingham, J.M. Seismic rocking simulation of unreinforced masonry parapets and façades using the discrete element method. *Earthq. Eng. Struct. Dyn.* **2022**, *51*, 1840–1856. [CrossRef]
32. Scattarreggia, N.; Malomo, D.; DeJong, M.J. A new Distinct Element meso-model for simulating the rocking-dominated seismic response of RC columns. *Earthq. Eng. Struct. Dyn.* **2023**, *52*, 828–838. [CrossRef]
33. Vlachakis, G.; Giouvanidis, A.I.; Mehrotra, A.; Lourenço, P.B. Numerical Block-Based Simulation of Rocking Structures Using a Novel Universal Viscous Damping Model. *J. Eng. Mech.* **2021**, *147*, 04021089. [CrossRef]
34. Ishiyama, Y. Motions of rigid bodies and criteria for overturning by earthquake excitations. *Earthq. Eng. Struct. Dyn.* **1982**, *10*, 635–650. [CrossRef]
35. Kaneko, M.; Hayashi, Y. Overturning criteria and horizontal displacements of rigid bodies to earthquake excitations. *J. Struct. Eng. Archit. Inst. Jpn.* **1997**, *43*, 451–458.
36. Kaneko, M.; Hayashi, Y. A proposal for simple equations to express a relation between overturning ratios of rigid bodies and input excitations. In Proceedings of the 13th World Conference on Earthquake Engineering, Vancouver, Canada, 1–6 August 2004; p. 14.
37. Kuo, K.C.; Suzuki, Y.; Katsuragi, S.; Yao, G.C. Shake table tests on clutter levels of typical medicine shelves and contents subjected to earthquakes. *Earthq. Eng. Struct. Dyn.* **2011**, *40*, 1367–1386. [CrossRef]
38. Zhang, J.; Makris, N. Rocking response of freestanding blocks under cycloidal pulses. *J. Eng. Mech.* **2001**, *127*, 473–483.
39. Thiers-Moggia, R.; Málaga-Chuquitaype, C. Dynamic response of post-tensioned rocking structures with inerters. *Int. J. Mech. Sci.* **2020**, *187*, 105927. [CrossRef]
40. Fragiadakis, M.; Psycharis, I.; Cao, Y.; Mavroeidis, G.P. Parametric investigation of the dynamic response of rigid blocks subjected to synthetic near-source ground motion records. In Proceedings of the ECCOMAS Congress, Crete Island, Greece, 5–10 June 2016; pp. 5–10.
41. Aslam, M.; Godden, W.G.; Scalise, D.T. Earthquake rocking response of rigid bodies. *ASCE J. Struct. Div.* **1980**, *106*, 377–392. [CrossRef]
42. Yim, C.-S.; Chopra, A.K.; Penzien, J. Rocking response of rigid blocks to earthquakes. *Earthq. Eng. Struct. Dyn.* **1980**, *8*, 565–587. [CrossRef]
43. Ibarra, L. *Seismic Performance of Dry Casks Storage for Long-Term Exposure*; NEUP 12-3756 Final Report; Nuclear Energy University Programs/University of Utah: Salt Lake City, UT, USA, 2016.
44. Bachmann, J.A.; Strand, M.; Vassiliou, M.F.; Broccardo, M.; Stojadinović, B. Is rocking motion predictable? *Earthq. Eng. Struct. Dyn.* **2018**, *47*, 535–552. [CrossRef]
45. Giannini, R.; Masiani, R. Risposta in frequenza del blocco rigido: Stabilita delle soluzioni. In Proceedings of the 10th Italian Association of Theoretical and Applied Mechanics, Rome, Italy, 15–19 September 2019.
46. Acikgoz, S.; Ma, Q.; Palermo, A.; DeJong, M.J. Experimental Identification of the Dynamic Characteristics of a Flexible Rocking Structure. *J. Earthq. Eng.* **2016**, *20*, 1199–1221. [CrossRef]
47. Cosenza, E.; Di Sarno, L.; Maddaloni, G.; Magliulo, G.; Petrone, C.; Prota, A. Shake table tests for the seismic fragility evaluation of hospital rooms. *Earthq. Eng. Struct. Dyn.* **2015**, *44*, 23–40. [CrossRef]
48. Feng, M.Q.; Shinozuka, M.; Kim, H.K.; Kim, S.H. Statistical analysis of fragility curves. *J. Eng. Mech.* **2000**, *126*, 1224–1231.
49. Roh, H.; Cimellaro, G.P. Seismic Fragility Evaluation of RC Frame Structures Retrofitted with Controlled Concrete Rocking Column and Damping Technique. *J. Earthq. Eng.* **2011**, *15*, 1069–1082. [CrossRef]

50. Deng, L.; Kutter, B.L.; Kunnath, S.K. Probabilistic Seismic Performance of Rocking-Foundation and Hinging-Column Bridges. *Earthq. Spectra* **2012**, *28*, 1423–1446. [CrossRef]
51. Kim, J.; Lorenzoni, F.; Salvalaggio, M.; Valluzzi, M.R. Seismic vulnerability assessment of free-standing massive masonry columns by the 3D Discrete Element Method. *Eng. Struct.* **2021**, *246*, 113004. [CrossRef]
52. Wagner, M.E.; Wittich, C.E.; Saifullah, M.K. Proficient Vector-Valued Intensity Measures for Overturning of Multi-Modal Three-Dimensional Freestanding Structures. In Proceedings of the 12th National Conference on Earthquake Engineering, Salt Lake City, UT, USA, 27 June–1 July 2022.
53. Giouvanidis, A.I.; Dimitrakopoulos, E.G. Rocking amplification and strong-motion duration. *Earthq. Eng. Struct. Dyn.* **2018**, *47*, 2094–2116. [CrossRef]
54. Liu, P.; Xue, W.; Pang, H.; Zhang, Y.M.; Chen, H.T.; Yang, W.G. Seismic overturning fragility analysis for freestanding building contents subjected to horizontal bidirectional floor motions. *Soil Dyn. Earthq. Eng.* **2022**, *161*, 107414. [CrossRef]
55. Lachanas, C.G.; Vamvatsikos, D. Rocking incremental dynamic analysis. *Earthq. Eng. Struct. Dyn.* **2022**, *51*, 688–703. [CrossRef]
56. Dimitrakopoulos, E.G.; Paraskeva, T.S. Dimensionless fragility curves for rocking response to near-fault excitations. *Earthq. Eng. Struct. Dyn.* **2015**, *44*, 2015–2033. [CrossRef]
57. Petrone, C.; Di Sarno, L.; Magliulo, G.; Cosenza, E. Numerical modelling and fragility assessment of typical freestanding building contents. *Bull. Earthq. Eng.* **2017**, *15*, 1609–1633. [CrossRef]
58. Sieber, M.; Vassiliou, M.F.; Anastasopoulos, I. Intensity measures, fragility analysis and dimensionality reduction of rocking under far-field ground motions. *Earthq. Eng. Struct. Dyn.* **2022**, *51*, 3639–3657. [CrossRef]
59. Liu, H.; Huang, Y.; Liu, X. An Intensity Measure for the Rocking Fragility Analysis of Rigid Blocks Subjected to Floor Motions. *Sustainability* **2023**, *15*, 2418. [CrossRef]
60. Liu, H.; Huang, Y.; Qu, Z. A discretely damped SDOF model for the rocking response of freestanding blocks. *Earthq. Eng. Eng. Vib.* **2022**, *21*, 729–740. [CrossRef]
61. Diamantopoulos, S.; Fragiadakis, M. Seismic response assessment of rocking systems using single degree-of-freedom oscillators. *Earthq. Eng. Struct. Dyn.* **2019**, *48*, 689–708. [CrossRef]
62. Weir, G.; McGavin, P. The coefficient of restitution for the idealized impact of a spherical, nano-scale particle on a rigid plane. *Proc. R. Soc. A: Math. Phys. Eng. Sci.* **2008**, *464*, 1295–1307. [CrossRef]
63. McKenna, F. OpenSees: A Framework for Earthquake Engineering Simulation. *Comput. Sci. Eng.* **2011**, *13*, 58–66. [CrossRef]
64. Nasi, K.T.J. *Stability of Rocking Structures*; Purdue University: Hammond, IN, USA, 2011.
65. Klaboe, K.; Pujol, S.; Laughery, L. *Stability of Rocking Structures*; Purdue University Research Repository: Hammond, IN, USA, 2017. [CrossRef]
66. Klaboe, K.; Pujol, S.; Laughery, L. Seismic Response of Rocking Blocks. *Earthq. Spectra* **2018**, *34*, 1051–1063. Available online: https://datacenterhub.org/resources/14255 (accessed on 20 December 2022). [CrossRef]
67. D'Angela, D.; Magliulo, G.; Cosenza, E. Seismic damage assessment of unanchored nonstructural components taking into account the building response. *Struct. Saf.* **2021**, *93*, 102126. [CrossRef]
68. Taghavi, S.; Miranda, E. Approximate Floor Acceleration Demands in Multistory Buildings. II: Applications. *J. Struct. Eng.* **2005**, *131*, 212–220. [CrossRef]
69. Huang, Y.; Beck, J.L.; Li, H. Bayesian system identification based on hierarchical sparse Bayesian learning and Gibbs sampling with application to structural damage assessment. *Comput. Methods Appl. Mech. Eng.* **2017**, *318*, 382–411. [CrossRef]
70. Linde, S.A.; Konstantinidis, D.; Tait, M.J. Rocking response of unanchored building contents considering horizontal and vertical excitation. *J. Struct. Eng.* **2020**, *146*, 04020175. [CrossRef]
71. Dimitrakopoulos, E.G.; DeJong, M.J. Overturning of Retrofitted Rocking Structures under Pulse-Type Excitations. *J. Eng. Mech.* **2012**, *138*, 963–972. [CrossRef]
72. Gehl, P.; Seyedi, D.M.; Douglas, J. Vector-valued fragility functions for seismic risk evaluation. *Bull. Earthq. Eng.* **2012**, *11*, 365–384. [CrossRef]